
DRAFT

CMS Physics Analysis Summary

The content of this note is intended for CMS internal use and distribution only

2010/07/19

Head Id: 15100

Archive Id: 15368M

Archive Date: 2010/07/17

Archive Tag: trunk

Search for Dijet Resonances in the Dijet Mass Distribution in pp Collisions at $\sqrt{s} = 7$ TeV

The CMS Collaboration

Abstract

We present a measurement of the dijet invariant mass spectrum and search for new particles decaying to dijets at CMS in pp collisions at $\sqrt{s} = 7$ TeV with 120 ± 13 nb⁻¹ of data. The dijet mass distribution of the two leading jets in the pseudorapidity region $|\eta| < 1.3$ is measured and compared to QCD predictions from PYTHIA propagated through the CMS detector simulation. The highest observed dijet mass is 2.13 TeV. We fit the observed dijet mass spectrum with a parameterization, search for dijet resonances, and set upper limits at 95% Confidence Level (C.L.) on the resonance cross section. These generic cross section limits are compared with theoretical predictions for the cross section for several models of new particles: string resonances, axigluons, colorons, excited quarks, E_6 diquarks, Randall-Sundrum Gravitons, W' and Z' . We exclude at 95% C.L. string resonances with mass less than 1.67 TeV, excited quarks with mass less than 0.59 TeV and axigluons and colorons with mass less than 0.52 TeV. Our limit on string resonances is more stringent than previously published limits.

This box is only visible in draft mode. Please make sure the values below make sense.

PDFAuthor:	Dijet Group
PDFTitle:	Search for Dijet Resonances in the Dijet Mass Distribution in pp Collisions at $\sqrt{s}=7$ TeV
PDFSubject:	CMS
PDFKeywords:	CMS, physics, software, computing

Please also verify that the abstract does not use any user defined symbols

1 Introduction

Within the Standard Model, events with two energetic jets (dijets) arise in proton-proton collisions from parton-parton scattering. The outgoing scattered partons manifest themselves as hadronic jets. The dijet mass spectrum predicted by Quantum Chromodynamics (QCD) falls smoothly and steeply with increasing dijet mass. Many extensions of the Standard Model predict the existence of new massive objects that couple to quarks (q) and gluons (g), and result in resonant structures in the dijet mass spectrum. In this paper we report a search for narrow resonances in the dijet mass spectrum, measured with the Compact Muon Solenoid (CMS) detector [1] at the CERN Large Hadron Collider, at a proton-proton collision energy of $\sqrt{s} = 7$ TeV.

In addition to this generic search, we search for manifestations of specific models of narrow dijet resonances. The following seven models provide specific predictions of the parton content of the dijet final state and the corresponding cross sections and branching fraction(s) as function of dijet mass. First, the model with the largest cross section is a recent model of string resonances, Regge excitations of the quarks and gluons in string theory, which includes resonances in all parton-parton channels ($q\bar{q}$, qq , gg and qg) with multiple spin states and quantum numbers [2, 3]. Second, in a model where the symmetry group $SU(3)$ of QCD is replaced by the chiral symmetry $SU(3)_L \times SU(3)_R$, there are axial vector particles called axigluons A , which decay to $q\bar{q}$ [4]. Third, the flavor-universal coloron model also embeds the $SU(3)$ of QCD in a larger gauge group, and predicts the presence of a color-octet coloron C , which decays to $q\bar{q}$ [5]. Fourth, if quarks are composite particles then excited states are expected, and we search for mass degenerate excited quarks q^* that decay to qg [6]. The compositeness scale is set to be equal to the mass of the excited quark. Fifth, grand unified theory based on the E_6 gauge group predicts the presence of scalar diquarks D and D^c , which decay to $\bar{q}\bar{q}$ and qq [7]. Sixth, the Randall-Sundrum (RS) model of extra dimensions predicts massive gravitons G , which decay to $q\bar{q}$ and gg [8]. For the RS graviton, the value of the dimensionless coupling κ/M_{Pl} is set to 0.1. And, finally, models that propose new gauge symmetries often predict new gauge bosons W' and Z' , which decay to $q\bar{q}$ [9]. The W' and Z' resonances are assumed to have standard model couplings and to have fractional widths equal to the corresponding standard model W and Z bosons. Table 1 summarizes some properties of these models. With the exception of the string resonances, the model parameters are in Reference [10].

2 Experimental Description

A detailed description of the CMS experiment can be found elsewhere [1]. The CMS coordinate system has the origin at the center of the detector, the z -axis points along the direction of the counterclockwise circulating proton beam of the LHC, with the transverse plane perpendicular to the beam. We define ϕ to be the azimuthal angle, θ to be the polar angle and the pseudorapidity as $\eta \equiv -\ln(\tan[\theta/2])$. The central feature of the CMS apparatus is a superconducting solenoid, of 6 m internal diameter, operating with a central field strength of 3.8 T. Within the field volume are the silicon pixel and strip tracker, and the barrel and endcap calorimeters ($|\eta| < 3$): a high granularity $PbWO_4$ crystal electromagnetic calorimeter (ECAL) followed by a brass-scintillator hadronic calorimeter (HCAL). Outside the field volume, in the forward region, there is an iron-quartz-fiber hadronic calorimeter ($3 < |\eta| < 5$). The ECAL and HCAL cells are grouped into towers, projecting radially outward from the origin, for triggering purposes and to facilitate the jet reconstruction. In the region $|\eta| < 1.74$ these projective calorimeter towers have segmentation $\Delta\eta = \Delta\phi = 0.087$, and the η and ϕ width progressively increases at higher values of η . The energy in the ECAL and HCAL within each projective tower is summed to find the calorimeter tower energy. Towers with $|\eta| < 1.3$ contain only cells

47 from the barrel calorimeters.

48 The data analyzed in this paper were collected in 2010 at a center-of-mass energy of 7 TeV.
 49 Non-collisional background is removed from the data sample and data quality cuts are applied
 50 to these data. The integrated luminosity of the selected data sample used for this analysis is
 51 $120 \pm 13 \text{ nb}^{-1}$. A single-jet trigger is applied in the online software-level trigger system, known
 52 as the High-Level Trigger (HLT), to select an unprescaled sample of events for this analysis. A
 53 parallel single-jet trigger with a lower p_T threshold is recorded with a prescaling of events for
 54 the purpose of computing trigger efficiencies. The trigger efficiency versus dijet mass for this
 55 analysis is measured from the data and is found to be greater than 99% for dijet masses above
 56 330 GeV as shown in Fig. 1. This analysis includes all dijet mass data above a threshold of
 57 354 GeV. The chosen threshold is defined by the a priori binning determined by the dijet mass
 58 resolution and is synchronized to a concurrent analysis of the dijet centrality ratio [11].

59 For the comparison between data and simulation of the dijet mass spectrum predicted by the
 60 QCD interactions of the Standard Model, the PYTHIA v6 Monte Carlo [12] is used. The gener-
 61 erated Monte Carlo samples are processed through a full GEANT4 simulation [13] of the CMS
 62 detector. The same Monte Carlo and simulation tools are used to extract resonance shapes and
 63 signal detection efficiencies for narrow resonances in dijet final states of varying parton content,
 64 as discussed in more detail in the following section.

65 Jets are reconstructed using the anti- k_T algorithm [14] with cone size $R = \sqrt{(\Delta\eta)^2 + (\Delta\phi)^2} =$
 66 0.7 . The reconstructed jet energy, E , is defined as the scalar sum of the calorimeter tower ener-
 67 gies inside the jet. The jet momentum, \vec{p} , is the corresponding vector sum: $\vec{p} = \sum E_i \hat{u}_i$ with
 68 \hat{u}_i being the unit vector pointing from the origin to the energy deposition E_i inside the cone.
 69 The jet transverse momentum, p_T , is the component of \vec{p} in the transverse plane. The E and
 70 \vec{p} of a reconstructed jet are then corrected for the non-linear response of the calorimeter to a
 71 generated jet, using Monte Carlo simulation [15]. Generated jets come from applying the same
 72 jet algorithm to the Lorentz vectors of stable generated particles before detector simulation.
 73 The corrections are chosen so that, on average, the p_T of a corrected jet is equal to the p_T of the
 74 corresponding generated jet.

75 The dijet system is composed of the two jets with the highest p_T in an event (leading jets),
 76 and the dijet mass is given by $m = \sqrt{(E_1 + E_2)^2 - (\vec{p}_1 + \vec{p}_2)^2}$. We select events with at least
 77 two jets and require that both leading jets have pseudorapidity $|\eta| < 1.3$. To remove possible
 78 instrumental and non-collisional backgrounds in the selected sample, jets are required to have
 79 a minimum of 1% of their total energy detected in the ECAL, a minimum multiplicity of 2
 80 calorimeter cells, ECAL or HCAL, and a maximum of 98% of the total energy occurring in a
 81 single photodetection device of the hadron calorimeter readout. The latter criterion forces a
 82 coincidence of channels to contribute to the energy measurement. The jet identification criteria
 83 remove less than 0.3% of the events passing the pseudorapidity constraints and dijet mass
 84 threshold. Events are required to have a reconstructed primary vertex. The ratio of the missing
 85 transverse energy (\cancel{E}_T) and the scalar sum of the total transverse energy (ΣE_T) computed from
 86 the calorimeter towers with $|\eta| < 5.0$ is plotted in Fig. 2 for the selected sample of dijet events.
 87 The distribution of energy in the events is well balanced in the transverse plane and shows no
 88 evidence for background processes that would populate the $\cancel{E}_T/\Sigma E_T$ ratio plot in the region
 89 close to unity. The distribution of the $\Delta\phi$ of the two leading jets, also plotted in Fig. 2, shows
 90 that the selected dijets are back-to-back in ϕ .

91 The CMS luminosity measurements, as determined from the luminosity system [1], are com-
 92 mon to all analyses using the same data sample. This luminosity is measured [16] using signals
 93 from the forward hadronic calorimeter.

3 Search for Narrow Resonances in the Inclusive Dijet Final State

The experimental method to search for dijet resonances uses the dijet mass spectrum measured from the two leading jets in the data. The Standard Model predicts a smoothly falling dijet mass distribution. The shape of the dijet mass distribution is first compared with QCD predictions from PYTHIA v6 propagated through the full CMS detector simulation. Then, a smooth parameterization of the dijet mass data distribution is used to model the background prediction for the narrow resonance search. The dijet resonance shapes for generic di-parton resonances containing qq , qg and gg partons were simulated in the limit that the natural widths are negligible compared to the experimental resolution of the dijet mass measurement. Figure 3 shows the resonance shapes used for this search. If a dijet resonance exists, it should appear in the dijet mass spectrum as a resonance peak on top of a smooth background.

The measured dijet mass spectrum is shown in Fig. 4 and 5. The mass spectrum is defined by

$$\frac{d\sigma}{dm} = \frac{1}{\int Ldt} \frac{N_i}{\Delta m_i} \quad (1)$$

where m is the dijet mass, N_i is the number of events in the i -th dijet mass bin, and Δm_i is the width of the i -th dijet mass bin, and $\int Ldt$ is the integrated luminosity. In Fig. 4 the bin width is approximately the dijet mass resolution, and gradually increases as a function of mass. In Fig. 5 beyond a dijet mass of 1 TeV we use wider bins, to eliminate bins with no events, and plot the point at the correct dijet mass value for comparison with the QCD spectrum. The data are compared to a PYTHIA v6 QCD Monte Carlo prediction using the absolute normalization set by the PYTHIA v6 QCD cross section, full simulation of the detector and the measured integrated luminosity corresponding to this data sample.

The highest dijet mass observed in this data sample is 2.13 TeV. Event displays of the highest mass dijet event are shown in Fig. 7 and exhibit collimated calorimeter energy deposits and associated tracks.

Figure 6 shows the dijet mass spectrum from Fig. 4 compared to a parameterized fit to a smooth function. The parameterization chosen is

$$\frac{d\sigma}{dm} = \frac{P_0 \cdot (1 - m/\sqrt{s})^{P_1}}{m^{P_2}} \quad (2)$$

The ratio between the data and the smooth background fit is compared to simulated excited quark and string resonance signals in Fig. 8. There is no indication for the presence of peaks above the background fit at the current level of data statistics.

4 Systematic Uncertainties

At the current level of integrated luminosity, only the largest sources of systematic uncertainties impact the narrow resonance search. These are given by:

- Jet Energy Scale (JES),
- Jet Energy Resolution (JER),
- Choice of Background Parameterization, and
- Luminosity.

We apply an uncertainty on JES of $\pm 10\%$ [15] and test the sensitivity of our analysis to a shift in the resonance signal by 10%, where a downward shift of the resonance mass encounters larger

128 QCD backgrounds and thus lowers the search sensitivity. The uncertainty on JER is estimated
 129 to be $\pm 10\%$. The JER uncertainty is applied to the expected signal shape, which is smeared
 130 with a Gaussian that increases the core resolution by 10%. Uncertainties in JER do not affect
 131 the background prediction as the background distribution is fit directly with data. For the back-
 132 ground parameterization, we consider an alternate 3-parameter functional form to fit the QCD
 133 background. Differences in the limit results using the alternate 3-parameter fit as compared to
 134 the default 3-parameter fit are used to estimate the systematic uncertainty on the background
 135 parameterization. In addition to the sources of uncertainty already mentioned, we include
 136 an uncertainty of 11% on the integrated luminosity [16]. To find the total systematics, we add
 137 the observed changes in quadrature. The individual and total systematic uncertainties as a
 138 function of resonance mass are illustrated in Fig. 9.

139 5 Results

For setting upper limits, before accounting for systematic uncertainties, we begin with a Bayesian formalism with uniform prior for the cross section. The likelihood as a function of a constant can be written as:

$$L = \prod_i \frac{\mu_i^{n_i} e^{-\mu_i}}{n_i!}, \quad (3)$$

where

$$\mu_i = \alpha N_i(S) + N_i(B), \quad (4)$$

140 n_i is the measured number of events in the i -th dijet mass bin, $N_i(S)$ is the number of events
 141 from signal in the i -th dijet mass bin, α is a parameter to multiply the signal and $N_i(B)$ is the
 142 number of expected events from background in the i -th dijet mass bin. For each dijet resonance
 143 mass and signal shape considered, the background in the i -th dijet mass bin, $N_i(B)$, is fixed to
 144 the value of the background parameterization that gives the best signal + background fit to the
 145 data. The number of signal events in the i -th dijet mass bin, $N_i(S)$, is the dijet resonance shape
 146 for qq , qg and gg resonances. The signal range is chosen to be asymmetric with the lower bound
 147 at $0.3m$ and the upper bound at $1.3m$, where m is the resonance mass. To incorporate systematic
 148 uncertainties, we use an approximate technique which in our application is generally more
 149 conservative than a fully Bayesian treatment. The posterior probability density for the cross
 150 section is broadened from that without systematic uncertainties by convoluting the likelihood
 151 distribution with a Gaussian systematic uncertainty for each resonance mass. As a result, the
 152 cross section limits including systematic uncertainties increase by 10%–37% as a function of
 153 resonance mass and type over the corresponding limits derived from statistical uncertainties
 154 alone.

155 The upper limits at 95% C.L. set on the cross section times branching ratio of centrally ($|\eta| <$
 156 1.3) produced dijet mass resonances are shown in Fig. 10. Separate limits are reported for dijets
 157 with three different parton contents, quark-quark (qq), quark-gluon (qg) and gluon-gluon (gg),
 158 in the final-state dijet system due to their differing resonance shapes. The limits are compared
 159 with calculations of the cross section times branching ratio for dijets in the fiducial acceptance
 160 $|\eta| < 1.3$ from the seven different models listed in Table 1. The fiducial acceptance of $|\eta| < 1.3$
 161 depends on the mass and spin of the resonance model, and ranges from 43% to 74% for an
 162 excited quark of mass between 0.5 TeV and 2.0 TeV, respectively. The cross section for string
 163 resonances, which decay predominantly to qg , can be compared to our upper limit on the cross
 164 section for qg resonances in Fig. 10. We exclude at 95% C.L. string resonances with mass less
 165 than 1.67 TeV, excited quarks with mass less than 0.59 TeV and axigluons and colorons of mass
 166 less than 0.52 TeV. For comparison, the cross section upper limits on dijet resonances from

167 the Tevatron [10] imply a limit on string resonances of about 1.4 TeV, and explicitly excluded
 168 excited quarks with mass less than 0.87 TeV and axiguons and colorons with mass less than
 169 1.25 TeV. The extrapolation of the current analysis sensitivity to higher integrated luminosities
 170 taken at $\sqrt{s} = 7$ TeV is in Reference [17], where Fig. 11 shows the expected mass limits for
 171 several models in the absence of a signal. With 0.4 pb^{-1} we anticipate reaching the Tevatron [10]
 172 exclusion for excited quarks.

173 6 Conclusion

174 A search for narrow resonances has been performed with the CMS experiment in the inclusive
 175 dijet final state using $120 \pm 13 \text{ nb}^{-1}$ of integrated luminosity taken at a center-of-mass of 7 TeV
 176 in proton-proton collisions at the LHC. We find that the dijet mass spectrum is a smoothly
 177 falling distribution in agreement with the predictions of the Standard Model. The highest dijet
 178 mass observed is 2.13 TeV, beyond the reach of the Tevatron. In the absence of any signifi-
 179 cant deviations from the shape of the expected background, upper limits at 95% C.L. are set
 180 on the cross section times branching ratio of centrally ($|\eta| < 1.3$) produced dijet mass reso-
 181 nances having natural widths negligible compared to the experimental resolutions. We have
 182 set mass limits on a few models of dijet resonances, including a mass limit of 1.67 TeV on string
 183 resonances which exceeds previous limits [10].

184 References

- 185 [1] CMS Collaboration, R. Adolphi et al., “The CMS experiment at the CERN LHC”, *JINST* **3**
 186 (2008) S08004. doi:10.1088/1748-0221/3/08/S08004.
- 187 [2] L. A. Anchordoqui et al., “Dijet signals for low mass strings at the LHC”, *Phys. Rev. Lett.*
 188 **101** (2008) 241803, arXiv:0808.0497. doi:10.1103/PhysRevLett.101.241803.
- 189 [3] S. Cullen, M. Perelstein, and M. E. Peskin, “TeV strings and collider probes of large extra
 190 dimensions”, *Phys. Rev.* **D62** (2000) 055012, arXiv:hep-ph/0001166.
 191 doi:10.1103/PhysRevD.62.055012.
- 192 [4] J. Bagger, C. Schmidt, and S. King, “Axiguon Production in Hadronic Collisions”, *Phys.*
 193 *Rev.* **D37** (1988) 1188.
- 194 [5] R. S. Chivukula, A. G. Cohen, and E. H. Simmons, “New Strong Interactions at the
 195 Tevatron?”, *Phys. Lett.* **B380** (1996) 92–98, arXiv:hep-ph/9603311.
- 196 [6] U. Baur, I. Hinchliffe, and D. Zeppenfeld, “Excited Quark Production at Hadron
 197 Colliders”, *Int. J. Mod. Phys.* **A2** (1987) 1285.
- 198 [7] J. L. Hewett and T. G. Rizzo, “Low-Energy Phenomenology of Superstring-Inspired E_6
 199 Models”, *Phys. Rept.* **183** (1989) 193.
- 200 [8] L. Randall and R. Sundrum, “Large Mass Hierarchy from a Small Extra Dimension”,
 201 *Phys. Rev. Lett.* **83** (1999) 3370.
- 202 [9] E. Eichten, I. Hinchliffe, K. D. Lane et al., “Super Collider Physics”, *Rev. Mod. Phys.* **56**
 203 (1984) 579–707.
- 204 [10] CDF Collaboration, T. Aaltonen et al., “Search for new particles decaying into dijets in
 205 proton- antiproton collisions at $\sqrt{s} = 1.96$ TeV”, *Phys. Rev.* **D79** (2009) 112002,
 206 arXiv:0812.4036. doi:10.1103/PhysRevD.79.112002.

- 207 [11] CMS Collaboration, “Search for New Physics in the Dijet Centrality Ratio”, CMS PAS
208 EXO-10-002.
- 209 [12] T. Sjostrand et al., “High-energy-physics event generation with PYTHIA 6.1”, *Comput.*
210 *Phys. Commun.* **135** (2001) 238–259, arXiv:hep-ph/0010017.
- 211 [13] GEANT4 Collaboration, S. Agostinelli et al., “GEANT4: A simulation toolkit”, *Nucl.*
212 *Instrum. Meth.* **A506** (2003) 250–303. doi:10.1016/S0168-9002(03)01368-8.
- 213 [14] M. Cacciari, G. P. Salam, and G. Soyez, “The anti- k_t jet clustering algorithm”, *Journal of*
214 *High Energy Physics* **2008** (2008), no. 04, 063.
- 215 [15] CMS Collaboration, “CMS Jet Performance in pp Collisions at $\sqrt{s} = 7$ TeV”, CMS PAS
216 JME-10-003.
- 217 [16] CMS Collaboration, “Measurement of CMS Luminosity”, CMS PAS EWK-10-004.
- 218 [17] CMS Collaboration, “The CMS physics reach for searches at 7 TeV”, CMS Note 2010/008.

DRAFT

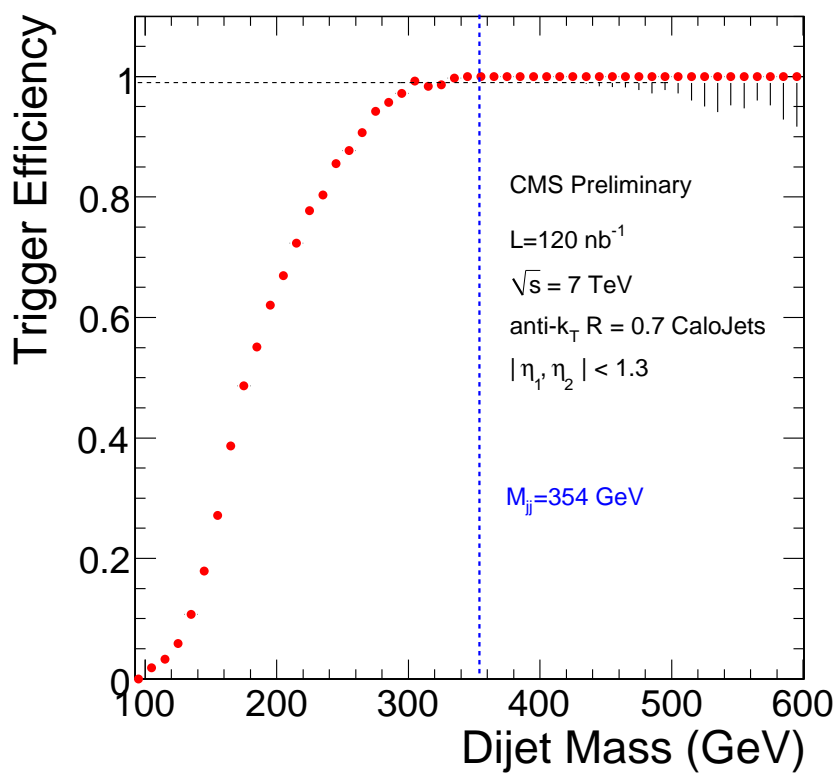


Figure 1: Trigger efficiency as a function of dijet mass for events with the two leading jets within a pseudorapidity of $|\eta| < 1.3$.

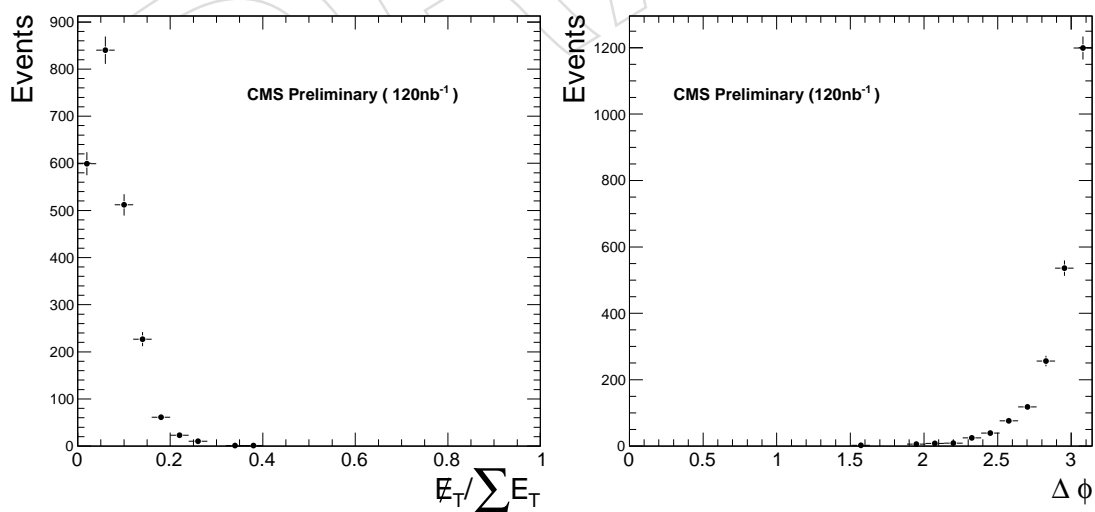


Figure 2: Left) Missing calorimeter E_T divided by total calorimeter E_T . Right) The phi difference of the two leading jets.

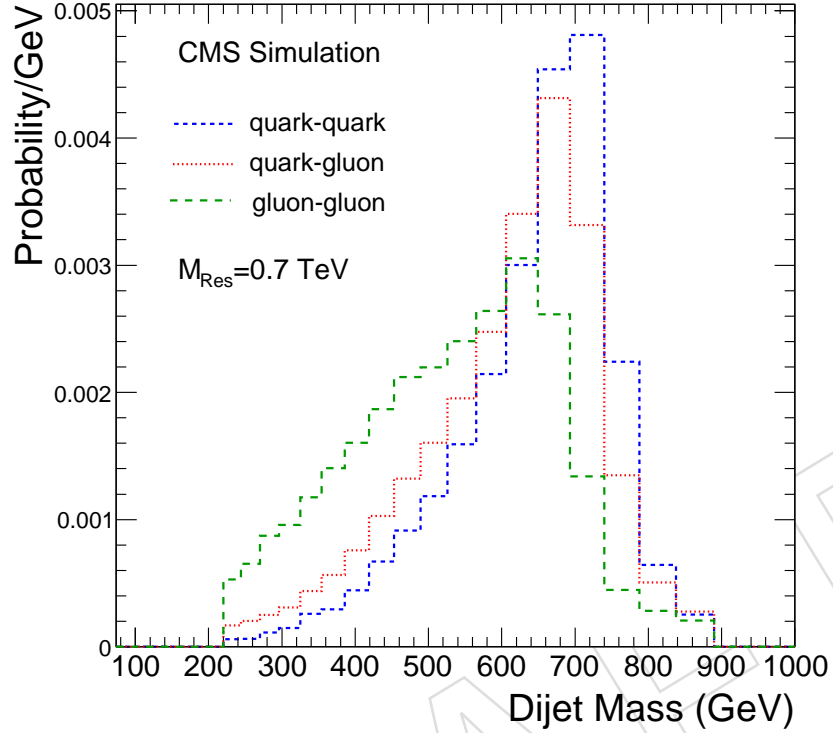


Figure 3: Expected signal shapes of dijet mass resonances for $q\bar{q}$ (qq), qg and gg resonances of mass 0.7 TeV as predicted from PYTHIA v6 Monte Carlo propagated through the full CMS detector simulation and jet reconstruction.

Model Name	X	Color	J^P	$\Gamma/(2M)$	Final-state Partons
String	S	mixed	mixed	0.003-0.037	$q\bar{q}$, qq , gg and qg
Axigluon	A	Octet	1^+	0.05	$q\bar{q}$
Coloron	C	Octet	1^-	0.05	$q\bar{q}$
Excited Quark	q^*	Triplet	$1/2^+$	0.02	qg
E_6 Diquark	D	Triplet	0^+	0.004	qq
RS Graviton	G	Singlet	2^+	0.01	$q\bar{q}$, gg
Heavy W	W'	Singlet	1^-	0.01	$q\bar{q}$
Heavy Z	Z'	Singlet	1^-	0.01	$q\bar{q}$

Table 1: Properties of Specific Dijet Resonance Models.

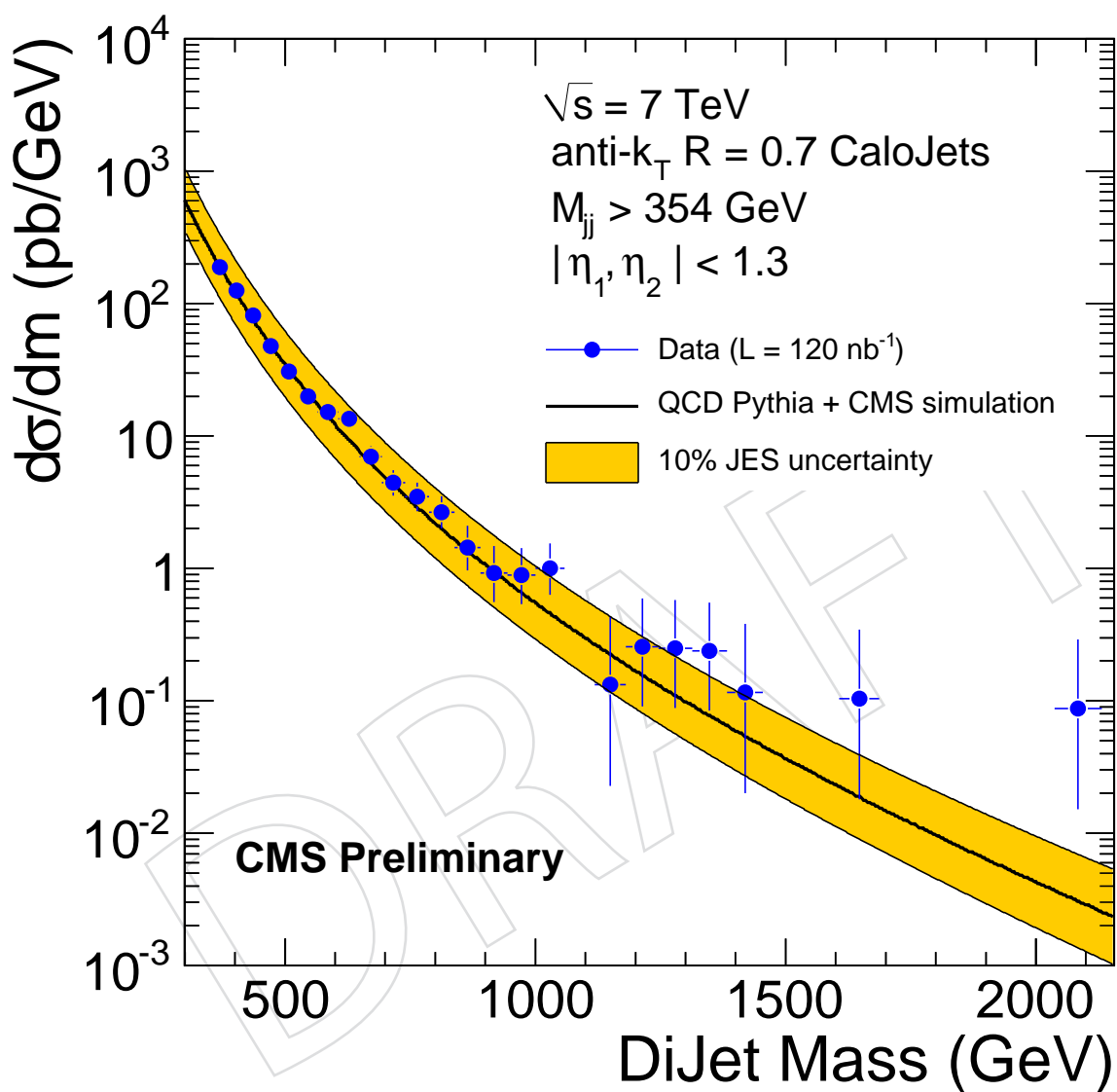


Figure 4: The measured differential cross section data (points) in dijet mass are compared to a QCD MC prediction (black line). The yellow band shows the sensitivity to a 10% systematic uncertainty on the jet energy scale.

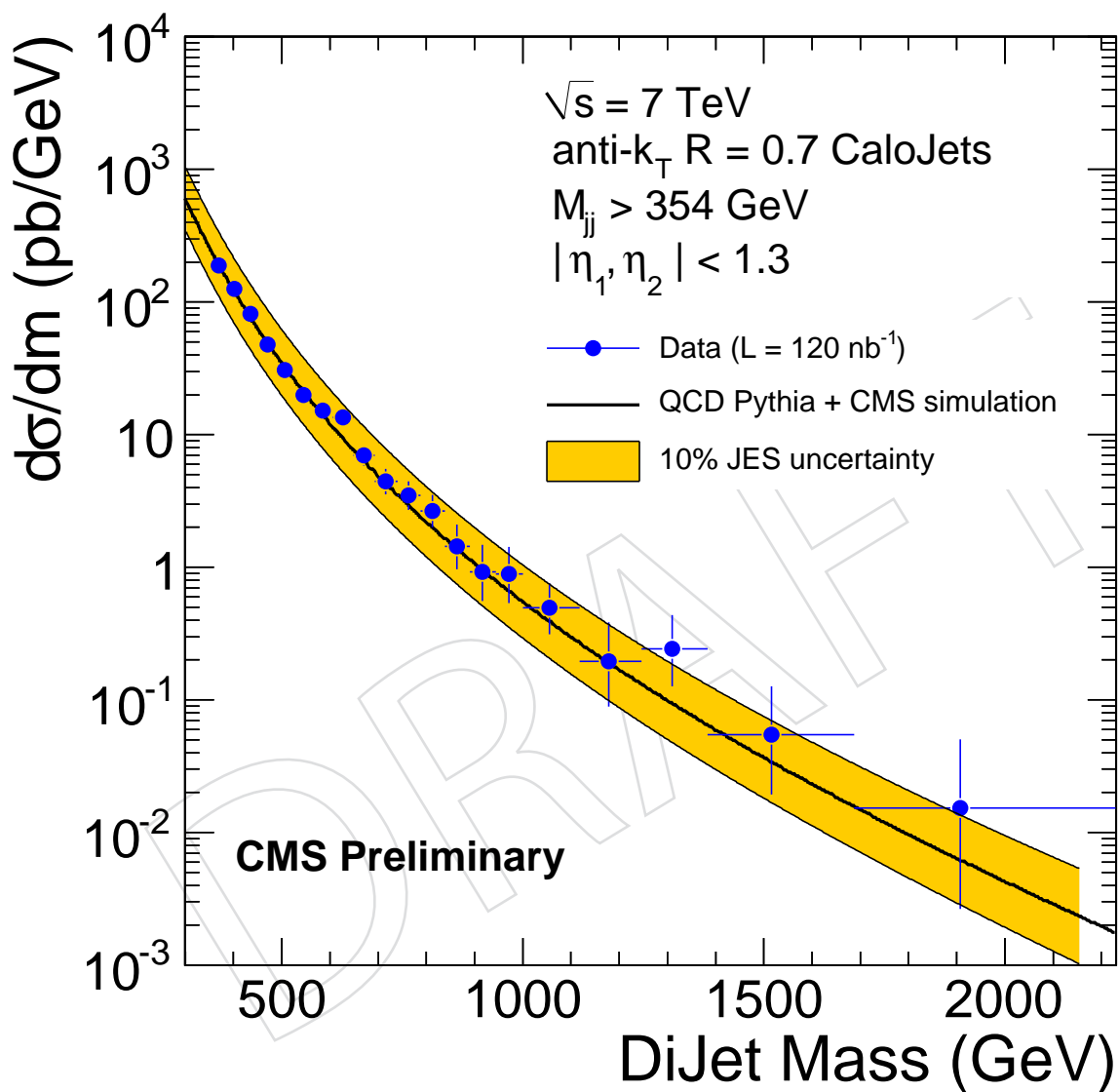


Figure 5: Same as Fig. 4 with coarser bins for dijet mass greater than 1 TeV.

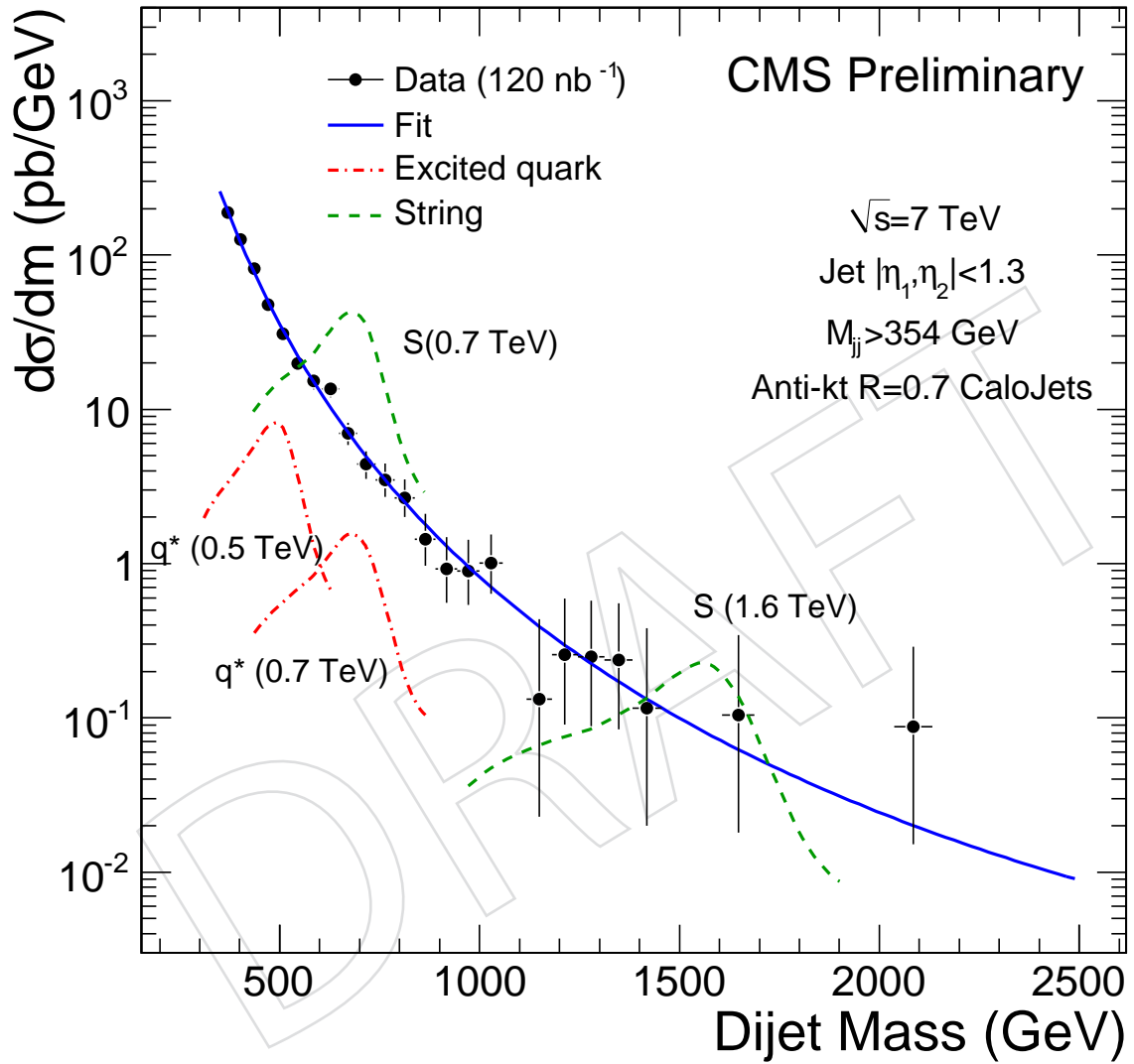


Figure 6: The dijet mass distribution (points) compared to simulations of excited quarks (dot-dashed red curves) and string resonance (green dashed curve) signals in the CMS detector.

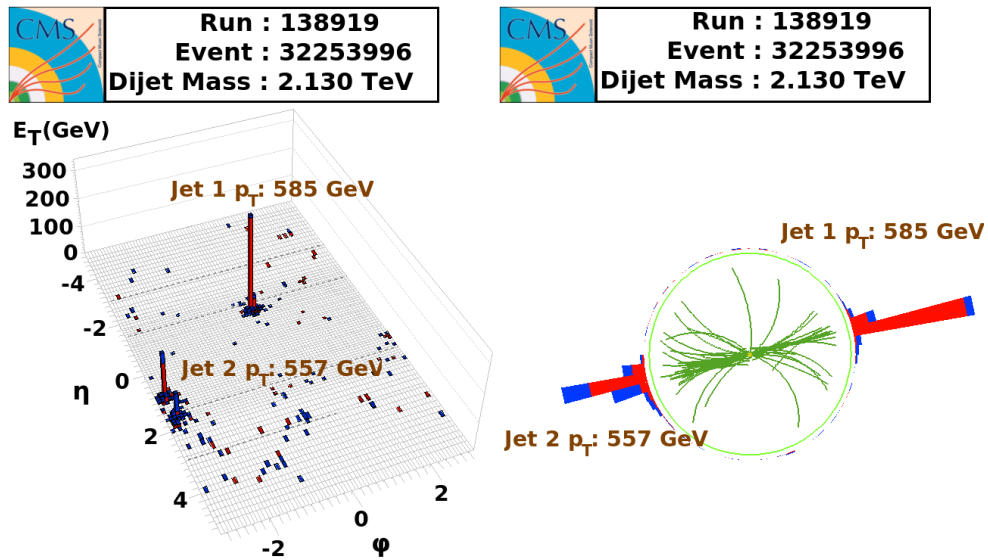


Figure 7: Lego display of calorimeter energies in η - ϕ coordinates (left) and in the transverse r - ϕ plane (right) of the highest mass dijet event. Jet 2 has two sub-jets separated in η at the same ϕ .

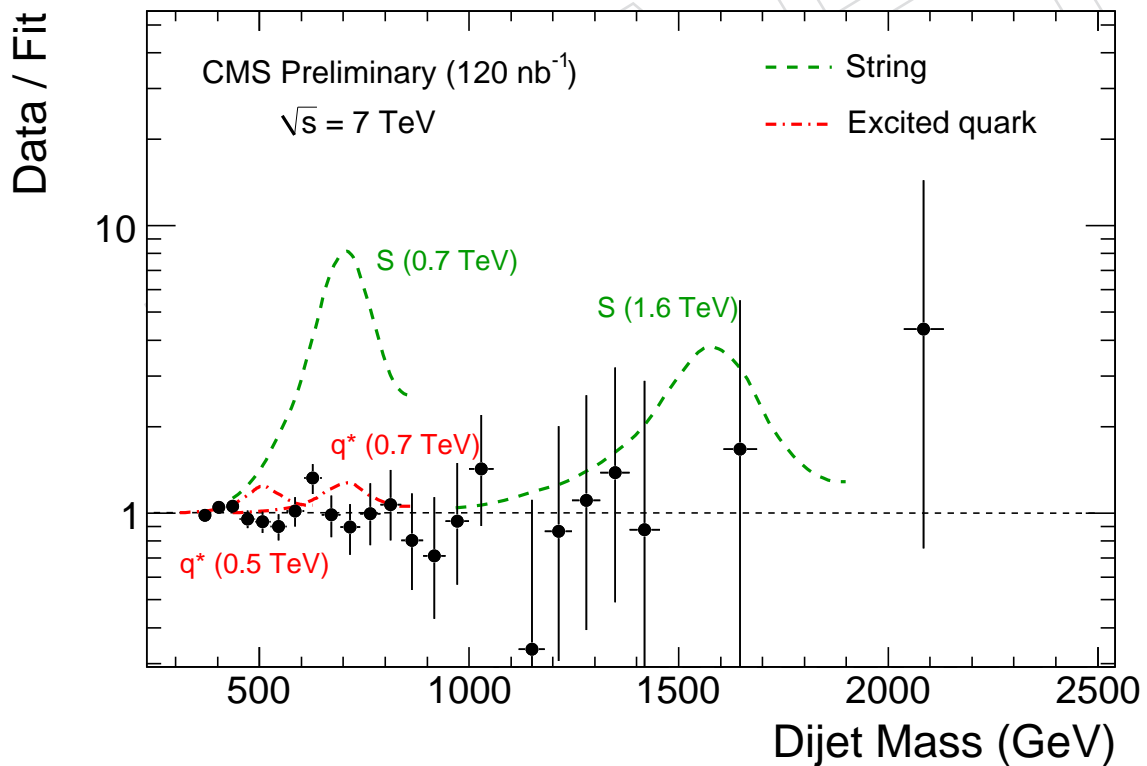


Figure 8: The ratio between the dijet mass distribution (points) and a smooth background fit (dashed line) is compared to a CMS detector simulation of an excited quark signal (dashed red curve) and a string resonance signal (dashed green curve).

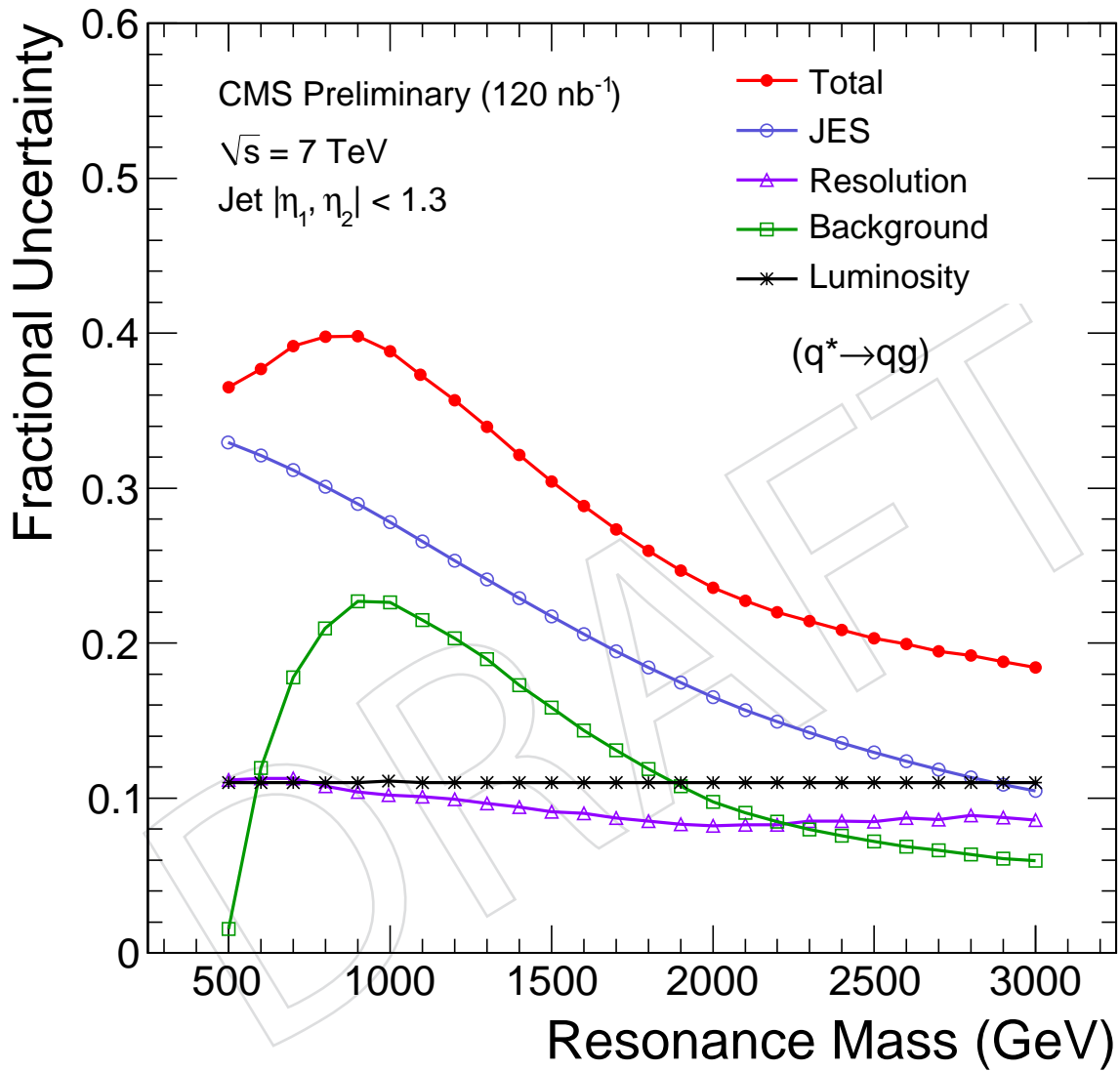


Figure 9: Fractional systematic uncertainties on the signal cross section showing the individual and total contributions for qg resonances.

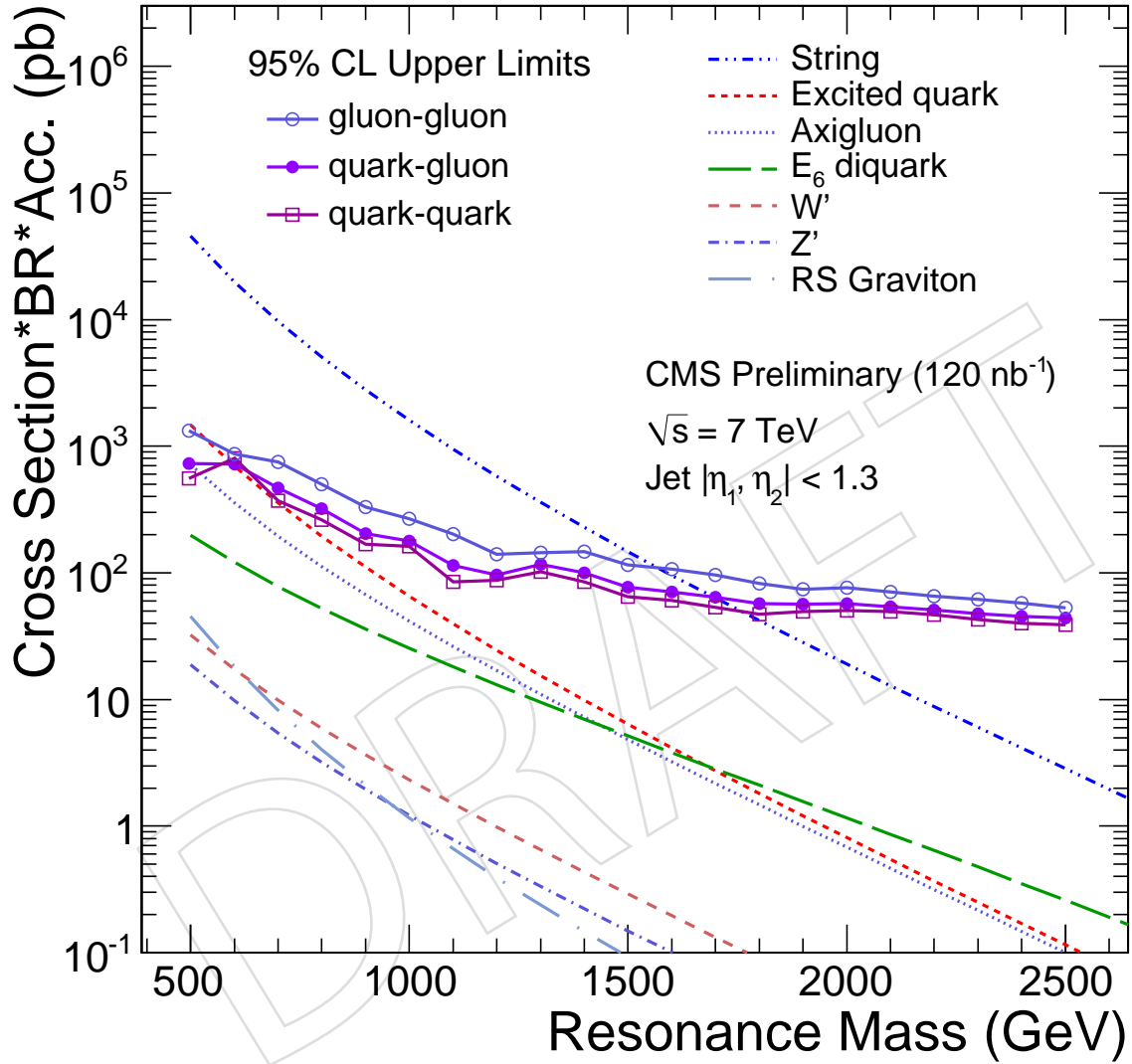


Figure 10: The 95% C.L. upper limits on the cross section for dijet resonances (points) shown separately for the three different parton pairs qq , qg and gg , is compared to cross section predictions for several new physics models.

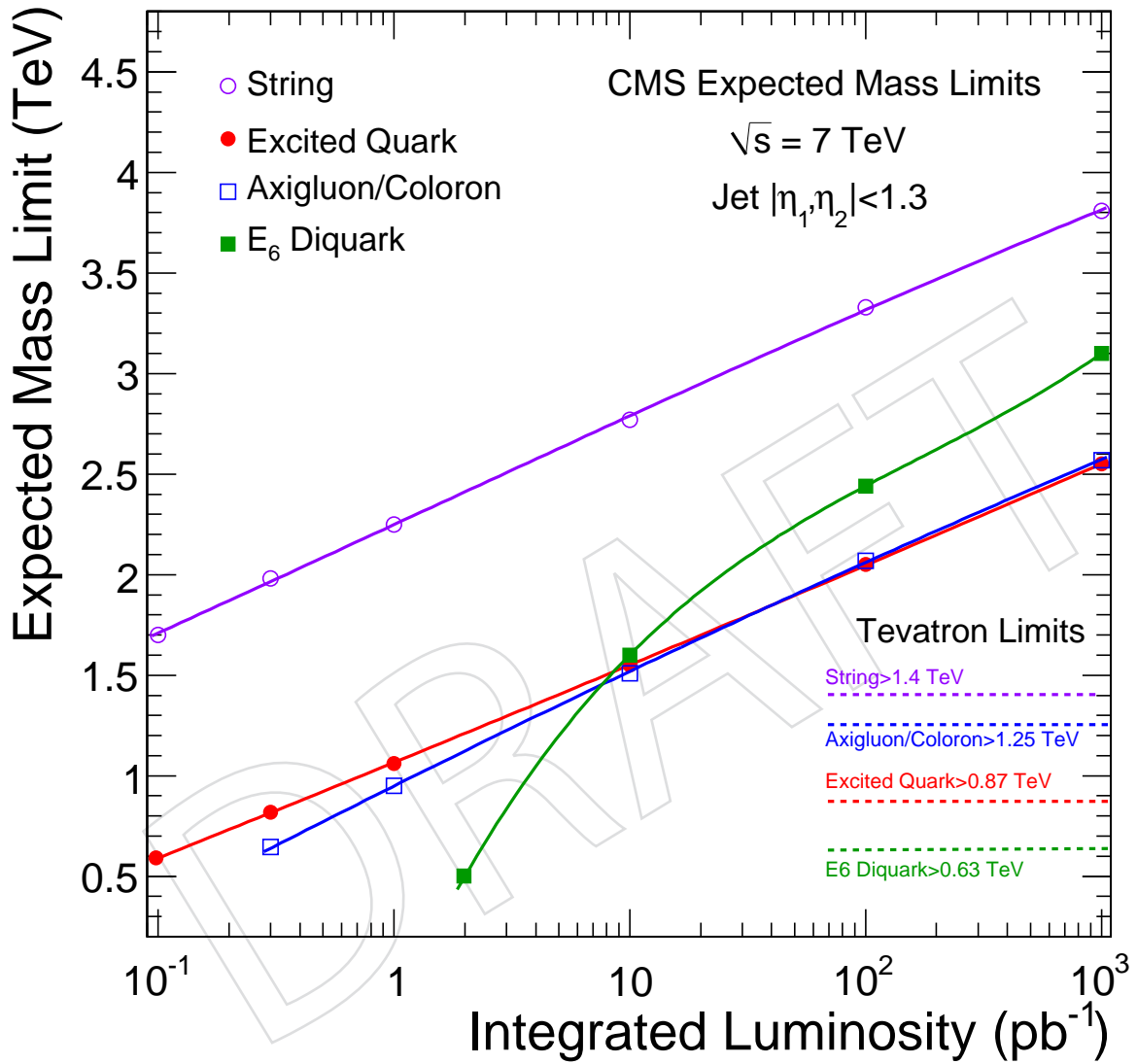


Figure 11: The expected mass limits for String, Excited Quark, Axigluon/Coloron and E_6 Diquark models of dijet resonances are plotted versus integrated luminosity and fit with a smooth curve.